Turbulence, Heat and Mass Transfer 10

Secondary motion impact on momentum and heat transfer in a fully developed turbulent channel flow.

A. Stroh, L. von Deyn, K. Schäfer, P. Forooghi and B. Frohnapfel
Institute of Fluid Mechanics (ISTM), Karlsruhe Institute of Technology (KIT), Kaiserstr. 10, 76131 Karlsruhe, Germany
stroh@kit.edu

Abstract – Surface structuring in form of streamwise-aligned triangular ridges is investigated in a DNS of a fully developed turbulent channel flow with constant wall temperatures of different values prescribed on the upper and lower walls at $\mathrm{Re}_\tau = 180, 500$ and 1000. Two arrangements of the ridges on both channel walls are considered – a symmetrical arrangement and a staggered arrangement with a spanwise shift of the upper wall structure by a half ridge-to-ridge separation. The ridges generate a strong large-scale secondary motion and hence enhance momentum and heat transfer in the channel. The composition of skin friction coefficient and Stanton number vary depending on Re_τ and structure arrangement from 7 to 32%. The component wise split-up of the Stanton number shows that staggered arrangement performs better in terms of heat transfer at higher Re_τ due to a more pronounced dispersive component.

1. Introduction

Secondary flows of Prandtl's second kind are known to be generated in turbulent boundary layer flows subjected to a spanwise inhomogeneity of the near-wall flow field [1]. The spanwise inhomogeneity alters local turbulent properties of the flow and introduces distinct gradients into the Reynolds stress distribution, which eventually manifests in the presence of large-scale vortex pairs occupying the entire boundary layer thickness and can significantly modify the mean velocity profile. [2]. The presence of secondary flow translates into an enhancement of momentum and heat transfer, which is of great interest from atmospherical, geological and technical point of view [3]. The present contribution presents a detailed analysis of the secondary flow generated in a channel with streamwise ridges and the related heat transfer.

2. Methodology

The analysis is carried out using flow fields produced by a direct numerical simulation (DNS) in a fully developed turbulent channel flow driven at a constant pressure gradient (CPG) corre-

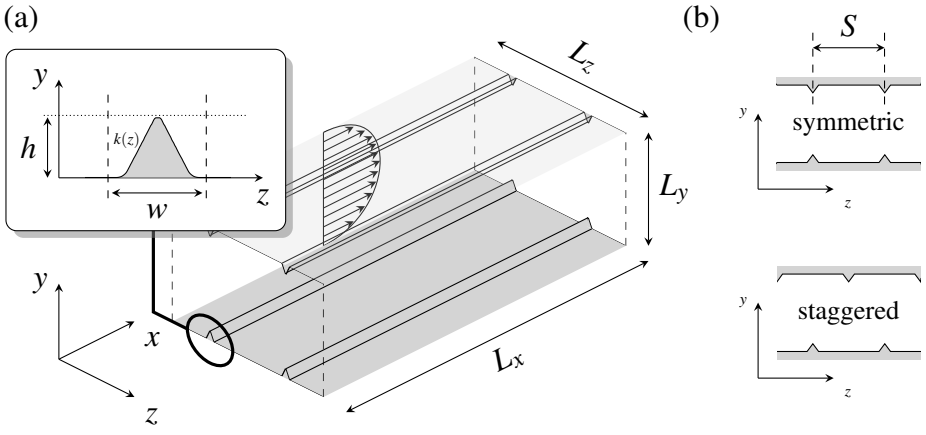

Figure 1: Schematic of (a) simulation domain, ridge geometry and (b) arrangements.

sponding to three friction Reynolds numbers $Re_\tau = u_\tau \delta_{eff}/\nu = 180, 500$ and 1000. The code implementation is based on the pseudo-spectral solver with Fourier expansions in the streamwise (x) and spanwise (z) directions and Chebyshev polynomials in the wall-normal direction (y) [4]. Periodic boundary conditions are applied for velocity field in the streamwise and spanwise directions, while the wall-normal extension of the domain is bounded by no-slip boundary conditions at the lower and upper domain wall ($y = 0, 2\delta$). Temperature is treated as a passive scalar with periodic boundary conditions applied for the thermal field in x- and z-directions, while a constant temperature on lower and upper wall is applied (T_l and T_u). This results in a fixed heat flux in the wall-normal direction. The Prandtl number is chosen to be $Pr = 0.71$, assuming air as the working fluid. The schematic of the numerical domain is depicted in Figure 1(a).

The elevated structures are placed on both channel walls in symmetric or staggered arrangement, where the structures on the upper wall are shifted in spanwise direction by half the element separation as shown in Figure 1 (b). The wall structuring is modeled by an immersed boundary method (IBM) through introduction of external volume force field to the Navier-Stokes equations [5]. The surface geometry of a streamwise-elongated triangular ridge is acquired using photogrammetry [6] from structured surface manufactured for an experimental investigation planned to be carried out in an open-circuit blower tunnel developed by Güttler [7]. The spacing between the ridges is given by $S = 1.752\delta$, while the height is $h = 0.16\delta$ and the width is $w = 0.22\delta$. The scanned structured surface and the evaluated height distribution $k(z)$ are shown in Figure 1 (a). Temporal and spatial averaging in the streamwise direction is applied to the DNS results, since the secondary motion is observed in the cross sectional plane perpendicular to the main flow direction.

3. Results

3.1 Secondary Motion

The magnitude of secondary motion and the flow topology is exemplary shown at $Re_\tau = 1000$ for staggered arrangement in Figure 2(a). It is confirmed that the large scale secondary flows are present in all configurations as reported by Stroh et al. [2]. Above the tips of the ridges the flow direction of the secondary motion is directed towards the channel center while a flow towards the channel walls is present in between the ridges. These wall-normal jets are very similar in their intensity distribution for both arrangements. However, in the symmetric arrangement two jets from the opposing walls impinge onto each other and introduce a stagnation point in the channel center (not shown here). For the staggered arrangement the jets emerging from the ridge tips reach the opposite wall. Therefore, we find streamlines that connect from the lower to the upper wall (and vice versa) for the staggered arrangement. We also confirm that the secondary flow topology for a particular structure arrangement remains very similar for all considered Re_τ.

3.2 Momentum and Heat Transfer

Table 1 summarizes the integral properties of the nine considered flow configurations. While the Re_τ is identically prescribed for the cases with ridges and the smooth-wall reference, the bulk mean velocity U_b is a result of the simulation. It decreases through the presence of the ridges since they introduce additional surface area and generate secondary motion. In consequence Re_b also drops.

The alteration of the skin friction coefficient and Stanton number relative to the smooth

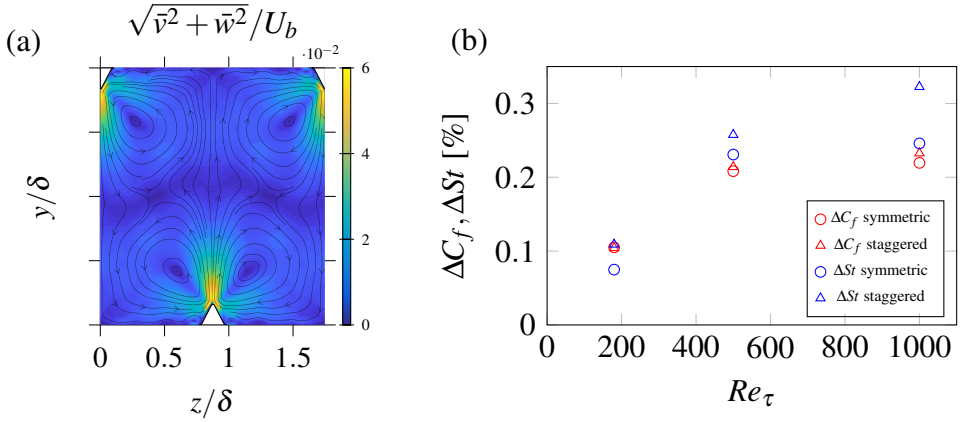

Figure 2: Secondary motion magnitude with streamlines at $Re_\tau = 1000$ in staggered arrangement (a) and increase of skin friction coefficient and Stanton number (b).

Re_τ	case	U_b^+	Re_b	C_f	Nu	St	RA	$\sqrt{\bar{v}^2+\bar{w}^2}/U_b$
180	smooth	15.73	5663	$8.08 \cdot 10^{-3}$	32.1	$3.99 \cdot 10^{-3}$	0.99	–
	symmetric	14.96	5387	$8.93 \cdot 10^{-3}$	32.8	$4.29 \cdot 10^{-3}$	0.96	4.6
	staggered	14.97	5389	$8.92 \cdot 10^{-3}$	33.9	$4.44 \cdot 10^{-3}$	0.99	4.5
500	smooth	17.99	18000	$6.17 \cdot 10^{-3}$	78.1	$3.06 \cdot 10^{-3}$	0.99	–
	symmetric	16.37	16375	$7.46 \cdot 10^{-3}$	87.5	$3.76 \cdot 10^{-3}$	1.00	5.6
	staggered	16.34	16336	$7.49 \cdot 10^{-3}$	89.2	$3.84 \cdot 10^{-3}$	1.00	5.7
1000	smooth	19.97	39941	$5.01 \cdot 10^{-3}$	145.5	$2.57 \cdot 10^{-3}$	1.02	–
	symmetric	18.08	36168	$6.12 \cdot 10^{-3}$	164.2	$3.20 \cdot 10^{-3}$	1.04	5.5
	staggered	17.99	35975	$6.18 \cdot 10^{-3}$	173.4	$3.39 \cdot 10^{-3}$	1.10	5.5

Table 1: Integral flow properties of the considered cases.

channel is shown in Figure 2(b). The increase of the skin friction coefficient ranges from 10% to 23% in comparison to the smooth channel depending on Reynolds number and structure arrangement. The analysis of the thermal field also shows an enhancement of the wall-normal heat transfer in the system. Interestingly, the Stanton numbers increase by 7.5% to 32% and its enhancement shows a more significant dependence on the structure arrangement than the enhancement of the skin friction coefficient, which barely changes for a particular Re_τ. This inevitably translates into a change of the Reynolds analogy factor between symmetric and staggered arrangements. In general, lower enhancement of St is observed for symmetric arrangements, while the increase is higher for staggered one. The highest variation between different arrangements is observed for $Re_\tau = 1000$, where St is increased by 25% or 32% for symmetric or staggered arrangement, respectively. This indicates that the presence of secondary flows might have a different impact on the heat transfer than on momentum in internal flows.

The triple decomposition [10] and FIK-identity split-up [11] allows an evaluation of the turbulent and dispersive (secondary motion related) contribution to the total heat flux at different Re_τ and arrangements. The contributions are shown in Figure 4. Symmetric arrangement (dashed lines) consistently shows a higher turbulent contribution, while the dispersive contribution is always higher for the staggered cases at all Re_τ. The figure shows a stronger enhancement of the dispersive component for staggered arrangement with growing Re_τ in comparison to the enhancement of turbulent contribution for symmetric arrangement. Since the sum of turbulent and dispersive parts mainly determines the total heat flux in the system, this translates into higher heat transfer coefficients for staggered arrangements at higher Re_τ.

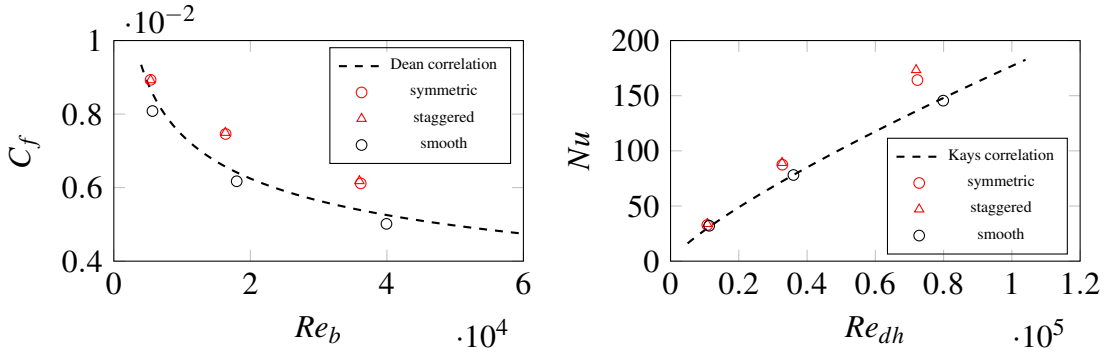

Figure 3: Skin friction coefficient and Nusselt number in symmetric and staggered arrangements at different Re compared to correlation by Dean [8] and Kays [9].

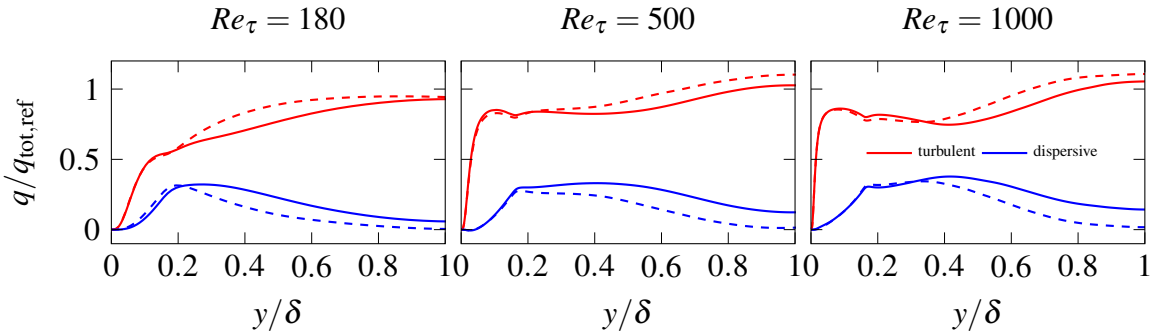

Figure 4: Turbulent and dispersive contribution to the total heat flux at different Re_τ in symmetric (dashed lines) and staggered (solid lines) arrangement.

4. Conclusions

A DNS study of a turbulent fully-developed flow over structured surfaces in two configurations (symmetric and staggered arrangement) is performed and compared to the smooth channel case. The presence of secondary motion significantly affects momentum and heat transfer properties of the flow. The results suggest that for the heat flux, both dispersive and turbulent contributions are mutually affected by the secondary flow topology, which are in turn controlled by the arrangement of the surface structures. It is found that the staggered arrangement enhances dispersive heat flux contribution more than the symmetric arrangement enhances the turbulent one at higher Re_τ. This translates into the better overall heat transfer performance for staggered arrangement and higher Reynolds numbers.

References

[1] P. Bradshaw. Turbulent secondary flows. *Annu. Rev. Fluid Mech.*, 19(1):53–74, 1987.

[2] A. Stroh, K. Schäfer, B. Frohnapfel, and P. Forooghi. Rearrangement of secondary flow over spanwise heterogeneous roughness. *J. Fluid Mech.*, 885:R5, 2020.

[3] Z.-Q. Wang and N.-S. Cheng. Time-mean structure of secondary flows in open channel with longitudinal bedforms. *Adv. Water Resour.*, 29(11):1634–1649, 2006.

[4] M. Chevalier, P. Schlatter, A. Lundbladh, and D. S. Henningson. Simson – A pseudo-spectral solver for incompressible boundary layer flows. Technical Report TRITA-MEK 2007-07, KTH Stockholm, Stockholm, Sweden, 2007.

[5] D. Goldstein, R. Handler, and L. Sirovich. Modeling a no-slip flow boundary with an external force field. *J. Comput. Phys.*, 105(2):354–366, 1993.

[6] B. Hallert. *Photogrammetry, basic principles and general survey*. McGraw-Hill, 1960.

[7] A. Güttler. *High accuracy determination of skin friction differences in an air channel flow based on pressure drop measurements*. PhD thesis, Karlsruhe Institute of Technology, 2015.

[8] R. B. Dean. Reynolds Number Dependence of Skin Friction and Other Bulk Flow Variables in Two-Dimensional Rectangular Duct Flow. *J. Fluids Eng.*, 100(2):215–223, 06 1978.

[9] W. M. Kays, M. E. Crawford, and B. Weigand. *Convective heat and mass transfer*, volume 76. McGraw-Hill Higher Education Boston, 2005.

[10] W. Reynolds and A. Hussain. The mechanics of an organized wave in turbulent shear flow. Part 3. Theoretical models and comparisons with experiments. *J. Fluid Mech.*, 54(2):263–288, 1972.

[11] K. Fukagata, K. Iwamoto, and N. Kasagi. Contribution of Reynolds stress distribution to the skin friction in wall-bounded flows. *Phys. Fluids*, 14:L73–L76, 2002.